International Journal of Pharmaceutics 647 (2023) 123554

Contents lists available at ScienceDirect

International Journal of Pharmaceutics

journal homepage: www.elsevier.com/locate/ijpharm

Development of innovative electrospun nepafenac-loaded nanofibers-based ophthalmic inserts

Safaa Omer [a], Nándor Nagy [b], Emőke Szőcs [b], Szabina Kádár [c,d], Gergely Völgyi [d], Balázs Pinke [e], László Mészáros [e], Gábor Katona [f], Anna Vincze [g], Péter Dormán [h], Zoltán Zs. Nagy [h], György T. Balogh [d], Adrienn Kazsoki [a,*], Romána Zelkó [a,*]

[a] University Pharmacy Department of Pharmacy Administration, Semmelweis University, Hőgyes Endre Street 7-9, H-1092 Budapest, Hungary
[b] Department of Anatomy, Histology and Embryology Semmelweis University, Tűzoltó Street 58, H-1094 Budapest, Hungary
[c] Department of Organic Chemistry and Technology, Faculty of Chemical Technology and Biotechnology, Budapest University of Technology and Economics, Műegyetem Rkp. 3, H-1111 Budapest, Hungary
[d] Department of Pharmaceutical Chemistry, Semmelweis University, Hőgyes Endre Street 9, H-1092 Budapest, Hungary
[e] Department of Polymer Engineering, Faculty of Mechanical Engineering, Budapest University of Technology and Economics, Műegyetem Rkp. 3, H-1111 Budapest, Hungary
[f] Institute of Pharmaceutical Technology and Regulatory Affairs, University of Szeged, Eötvös u. 6, H-6720 Szeged, Hungary
[g] Department of Chemical and Environmental Process Engineering, Budapest University of Technology and Economics, Műegyetem Rkp. 3, H-1111 Budapest, Hungary
[h] Department of Ophthalmology, Semmelweis University, Ma´ria Street 39, 1085 Budapest, Hungary

ARTICLE INFO

Keywords:
Nepafenac-loaded formulations
Electrospun nanofiber-based ocular insert
Morphological and solid-state characterization
Cytocompatibility study
In vitro dissolution study
Accelerated stability test
Ex vivo permeability study

ABSTRACT

Electrospun nanofibers can be utilized to develop patient-centric ophthalmic formulations with reasonable bioavailability at the targeted site. The current study aimed to develop 0.1 % w/w of nepafenac-loaded electrospun nanofibrous webs as potential candidates for ocular delivery of nepafenac with improved solubility and stability. Nine different formulations were prepared by electrospinning and investigated for morphology, physicochemical properties, drug release, cytocompatibility, and in vitro and ex vivo permeability. The scanning electron microscopy images showed fibrous samples. Fourier transform infrared spectroscopy and X-ray diffraction confirmed the polymer cross-linking and the formation of amorphous solid dispersion. All formulations showed complete and fast release of nepafenac (≤60 min), and the release followed first-order kinetics (β values for all formulations were < 1). The formulations (F3, F6, and F9) showed considerable in vitro and ex vivo permeability. The Raman studies revealed comparable corneal distributions of F3 and the commercial Nevanac® suspension at 60 min (p value = 0.6433). The fibrous composition remains stable under stress conditions (40 ± 2 °C, 75 ± 5 % relative humidity). The formulation composition showed good cytocompatibility with hen eggs tested on the chorioallantoic membrane of chick embryos. The developed nanofiber webs could be a promising candidate for nepafenac-loaded ophthalmic inserts.

1. Introduction

Delivery of the drug to the eye is a complex process due to its unique structure. This unique structure consists of different anatomical and physiological layers and barriers that protect the eye from invasion by foreign objects and interfere with drug permeation (Chen et al., 2018; Maharjan et al., 2019; Mehta et al., 2017). The ever-increasing number of eye diseases can lead to socioeconomic difficulties and interfere with individuals' quality of life (Pascolini & Mariotti, 2012). Untreated patients may develop serious symptoms involving both the anterior and posterior segments; consequently, glaucoma, vision impairment, or even blindness can occur (Kaur et al., 2021; Liang et al., 2021; Pinxten et al., 2017).

Treatment of different ocular diseases is based on the utilization of conventional topical formulations. Eye drops are most popular among physicians and patients due to their convenient way of self-administration. However, because of the limitations of premature loss of the drug and limited bioavailability (less than 5 %) from such formulations, the therapeutic goal is only achieved through frequent administration (Maharjan et al., 2019). The intravitreal injection can be

* Corresponding authors.
E-mail addresses: kazsoki.adrienn@semmelweis.hu (A. Kazsoki), zelko.romana@semmelweis.hu (R. Zelkó).

https://doi.org/10.1016/j.ijpharm.2023.123554
Received 17 August 2023; Received in revised form 12 October 2023; Accepted 23 October 2023
Available online 30 October 2023

used successfully for site targeting, yet it is considered an invasive method, requires a skilled ophthalmologist, and may expose the individual to serious complications such as severe hemorrhage, retinal detachment, and blindness (Singla et al., 2019). Novel drug delivery systems comprise a successful and promising alternative to conventional formulations for site targeting. They are designed to increase the residence of the drug and/or improve drug permeation (Barse et al., 2017; Lakhani et al., 2020). These novel formulations include, but are not limited to, hydrogels, liposomes, nanoparticles, ophthalmic inserts, implants, contact lenses, nanosuspensions, and in situ gels (Tighsazzadeh et al., 2019).

Ophthalmic inserts (OIs) have received a great deal of attention due to their numerous advantages. They are fabricated from a wide range of polymers and excipients that can be utilized to increase the residence time, sustain the drug release, enhance transcorneal absorption, and consequently improve bioavailability. Because OIs are solid preparations, they are more stable compared to liquid formulations and eliminate the need for preservatives, thereby reducing the side effects and irritation arising from different preservatives (Di Prima et al., 2019; Polat et al., 2020a; Thakkar et al., 2021).

Electrospinning is one of the novel and promising methods that are used for the fabrication of ophthalmic inserts (Polat et al., 2020b). The method enables the encapsulation of one or more drugs and/or excipients in a single compartment. A more complex nanofibrous structure can be prepared and utilized to deliver incompatible and large drug molecules, including proteins and nucleic acids. The process enables easy surface engineering and modification using different materials such as permeation enhancers, solubility modifiers, and mucoadhesive polymers (Singla et al., 2019).

Polyvinyl alcohol (PVA) is a synthetic polymer that is widely used in the electrospinning process due to its desirable properties such as mechanical strength and biodegradability (Fan et al., 2019; Meireles et al., 2018). Poloxamers are tri-block copolymers consisting of repeated units of terminal hydrophilic ethylene oxide (EO) and central hydrophobic propylene oxide (PO) (Dumortier et al., 2006). They are considered a unique class of polymers due to their thermoreversible phenomenon and amphiphilic features that enable micelle formation and encapsulation of hydrophobic drugs while using an aqueous platform. Poloxamer 407 (Pluronic F127) is widely used in ophthalmic formulations to solubilize drugs and impart adhesiveness to the formulation (Dumortier et al., 2006; Galgatte & Chaudhari, 2014; Russo & Villa, 2019).

Cyclodextrins (CD) are a family of cyclic oligosaccharides with a hydrophobic core and hydrophilic shell. They can be used to form inclusion complexes with hydrophobic compounds to improve water solubility and stability (Grimaudo et al., 2018; MacHín et al., 2012; Miranda et al., 2021).Hydroxypropyl-β-cyclodextrin (HPβCD) is frequently utilized in ophthalmic formulations due to its low tendency to precipitate eye irritation (He et al., 2011).

Inflammatory eye diseases have a high incidence rate and affect both the anterior and posterior parts. Failure of the treatment can lead to visual impairment and blindness. Nepafenac is a non-steroidal anti-inflammatory drug approved by the FDA for the topical treatment of allergic conjunctivitis as well as post-operative pain and inflammation (Lorenzo-Veiga et al., 2020). It is a crystalline powder with low water solubility and low permeability (class IV) (Lorenzo-Veiga et al., 2019). Nepafenac is stable in solid form, while it tends to form degradation products in liquid formulations (Aleo et al., 2020). Nepafenac is normally used as a suspension because of its low water solubility. The suspensions have many limitations, such as irritation and unpleasant sensations that can lead to excessive loss of the drug through lacrimation; hence, frequent dosing is required, which can result in patient noncompliance and treatment failure that might eventually lead to blindness and social difficulties. To avoid these limitations, there is a need for topical formulations that have more tolerability and the ability to overcome the inherently defensive mechanisms of the eye layers (Di Prima et al., 2019; Polat et al., 2020a; Thakkar et al., 2021).

The current study aimed to develop and formulate electrospun nanofiber-based ophthalmic inserts for the delivery of nepafenac to find a stable, solid preservative-free formulation that can overcome premature drainage and increase patients' acceptability. The formulation uses PVA as a matrix-forming polymer, Poloxamer 407 to impart adhesiveness and form in situ gel, and HPβCD as a solubilizer and stabilizer.

2. Material and methods

2.1. Materials

Nepafenac (NEPA, a product of TCI Ltd. (Tokyo, Japan)). polyvinyl alcohol (PVA, Mowiol® 18–88 with an average molecular weight Mw ~ 130 kDa), poloxamer 407 (average molecular weight, Mw ~ 12.6 kDa), chloroform (anhydrous, ≥ 99 %), hexane (anhydrous, 95 %), dodecane (anhydrous, ≥ 99 %) and methanol (anhydrous, 99.8 %) were obtained from Merck Ltd. (Budapest, Hungary). L-α-phosphatidylcholine was purchased from Merck KGaA (Darmstadt, Germany). Hydroxypropyl-β-cyclodextrin (HPβCD) (average degree of substitution (n): 4.5, average molecular weight: 1135.0 + n × 58.1 g mol^{-1}) was purchased from Cyclolab Ltd. (Budapest, Hungary). Sodium chloride, sodium hydrogen carbonate, calcium chloride hexahydrate and Ethylenediaminetetraacetic acid (EDTA) were purchased from Molar Chemicals Ltd (Budapest, Hungary). Pharmacopeial-grade distilled water was used as solvent for precursor solution preparation. For the permeation experiments, distilled water was purified by the Millipore Milli-Q® 140 Gradient Water Purification System. For the ex vivo experiments, porcine eyes were obtained from a local slaughterhouse (Porció-ÉK Ltd., Albertirsa, Hungary). Physiological salt solution (PSS) contained 0.9 % NaCl (Hungaropharma Plc., Budapest, Hungary). All materials were used without further purification.

2.2. Methods

2.2.1. Preparation of Nepafenac/ HPβCD solution in water

The solubility of nepafenac in water in the presence of HPβCD has been conducted based on the results of the published report (Lorenzo-Veiga et al., 2019). 1 mg of nepafenac was added to 50 mM HPβCD aqueous solutions and subjected to heating in sealed vials at 60 °C for 60 min. The concentrations of resultant solutions were determined by measuring the absorbance at λ_{max} 238 nm by Jasco 530 UV–VIS spectrophotometer coupled with inline probe. The experiments were carried out in triplicate and the average amounts were determined based on the previously constructed calibration curve. The method of analysis was validated according to the reported work (Rajput et al., 2015; Wagh et al., 2017).

2.2.2. Preparation of electrospinning solutions

Variable amounts of HPβCD and PVA/poloxamer 407 were used to prepare nine different solutions of nepafenac (Table 1). The precursor solutions containing HPβCD to improve NEPA solubility; PVA as fiber

Table 1
Composition of nepafenac (NEPA)/hydroxypropyl-beta-cyclodextrin (HPβCD), loaded in different ratios of polyvinyl alcohol (PVA): Poloxamer 407.

Formulation Code	NEPA (% w/w)	HPβCD (mM)	PVA: Poloxamer 407 (m: m)
F1	0.1	50	100:00
F2	0.1	50	85:15
F3	0.1	50	80:20
F4	0.1	100	100:00
F5	0.1	100	85:15
F6	0.1	100	80:20
F7	0.1	150	100:00
F8	0.1	150	85:15
F9	0.1	150	80:20

forming polymer; and poloxamer 407 to impart the bio-adhesiveness. The individual solutions were prepared using appropriate amounts of polymers and distilled water. PVA solutions were prepared by dispersing the polymers in the distilled water, followed by stirring under heating until clear solutions were obtained. Poloxamer 407 solutions were prepared by dissolving the required amounts in cold water. PVA/poloxamer 407 solutions were prepared by adding poloxamer 407 solutions to the PVA solutions and stirred at room temperature until complete homogenization. NEPA/ HPβCD was added either to the PVA or PVA/poloxamer 407 solutions and subjected to stirring at 60 °C for 60 min followed by stirring at room temperature for 2 h until complete solubility of nepafenac.

2.2.3. Electrospinning of the solutions

The fiber formation was conducted using laboratory scale electrospinning equipment (SpinSplit Ltd., Budapest, Hungary). A plastic syringe (Luer lock syringe, Merck Ltd., Budapest, Hungary) of 1 mL volume was filled with the precursor solution and connected to conventional needle (22G) through a Teflon tube. The filled syringe was then placed on the pump to ensure persistent solution flow. Several preliminary experiments have been conducted to optimize the process parameters. The electrospinning process was set at flow rate of (0.08–0.1 μL/sec); the applied voltage was in a range of (10–20 kV); and the effective distance between the needle tip and the grounded collector was maintained at (10 cm, 12.5 cm, and 15 cm). An aluminum foil wrapped on the surface of the grounded plate collector was used to collect each individual sample. The samples were then stored in desiccator for subsequent analysis. Parameter combinations that provided the best sample morphology were used for further sample preparation. The process was conducted at ambient conditions of 22 ± 1 °C room temperature and 40 ± 5 % relative humidity.

2.2.4. Morphological characterization

Electrospun samples were subjected to morphological characterization using the scanning electron microscope (SEM) type JEOL JSM-6380LA. Samples were initially fixed to the copper ingots with double-sided carbon adhesive and coated with gold under vacuum. Images were captured at 3500 and 5000 magnifications at 10 mm distance and an acceleration voltage of 15 kV. Images taken were evaluated in terms of fibrous and beads containing samples. For all fibrous samples, the diameters of 100 randomly selected individual fibers (n = 100) were measured from two different images using ImageJ software (US National Institutes of Health, 138 Bethesda, MD, USA). The average fiber diameters and the standard deviations for all sample measurements were calculated using Excel 2010. The histograms and fitting to the gaussian (normal) distribution were conducted using OriginPro 2018 software (v9.5.1, OriginLab Corporation, Northampton, MA, USA). For assessing the normality of fiber diameter distribution, skewness and kurtosis have been calculated using Microsoft Excel 2010 functions based on the Equations (1) and (2):

$$Skew = \frac{n}{(n-1)(n-2)} \Sigma \left(\frac{xi - x}{s}\right)^2 \quad (1)$$

$$Curtosis = \frac{n}{(n-1)(n-2)(n-3)} \Sigma \left\{\left(\frac{xi - x}{s}\right)^4\right\} - \frac{3(n-1)^2}{(n-2)(n-3)} \quad (2)$$

2.2.5. Solid state characterization

2.2.5.1. Fourier transform infrared spectroscopy. Fourier transform infrared spectroscopy (FTIR) was used to investigate the physicochemical properties, compatibility, and interactions between polymers and other excipients using the Jasco FT/IR-4200 spectrophotometer (Jasco Inc., Easton, MD, USA). The analysis was performed for the physical forms of the individual components and the fibrous mixtures. The measurement was conducted in the 400–4000 cm^{-1} range at a resolution of 4 cm^{-1} at ambient temperature in an average of 100 scans.

2.2.5.2. X-ray diffraction (XRD). Diffraction patterns were measured on PANalytical X'Pert3 Powder diffractometer (Malvern Panalytical B.V., The Netherlands) using Cu Kα radiation with 45 kV accelerating voltage and 40 mA anode current over the range of 4–38 ° 2 θ with 0.0080 ° step size and 99.695 s times per step in reflection mode, spinning the sample holder by 1 s^{-1}. Incident beam optics were as following: Programmable divergence slit with 15 mm constant irradiated length, anti-scatter slit at fixed 2 °. Diffracted beam optics consisted of X'Celerator Scientific ultrafast line detector with 0.02 soller slit and programmable anti-scatter slit with 15 mm constant observed length. Data were collected by PANalytical Data Collector Application, version 5.5.0.505 (Malvern Panalytical B.V., The Netherlands).

2.2.6. Determination of the drug content

The nepafenac content of different fibers was determined by dissolving the amount required to produce a final concentration of 10 μg/mL in 10 mL phosphate-buffered saline (PBS) at pH 7.4 and stirring at ambient conditions for 120 min. The absorbance of the resultant solution was measured at λ_{max} 238 nm by a Jasco 530 UV–VIS spectrophotometer coupled with an inline probe. The experiment was carried out in triplicate and the average amounts were determined based on the previously constructed calibration curve.

2.2.7. In vitro release study and release kinetics

The in vitro release of nepafenac from electrospun nanofibers was studied using a modified method analogous to the basket method reported by Pharmacopoeia Hungarica (Ph.Hg. VIII) (Kazsoki et al., 2021). The method was adjusted to mimic small volume physiological compartments. The process was conducted in a 25-mL beaker. The weighed samples were folded on a dry magnetic bar and fixed inside a steel coil. The folded samples were then inserted inside the 25-mL beaker and magnetically stirred at 100 rpm at a temperature of 37 ± 0.5 °C. An inline probe of a spectrophotometer (Jasco-V-750 UV–VIS spectrophotometer) was immersed in the beaker for continuous measurement of the absorbance of the released nepafenac. 10 mL of pre-warmed phosphate buffer pH 7.4 (to 37 °C) was added to the sample (dissolution media), and the absorbances were measured at a predetermined time interval (5 s) at λ_{max} 238 nm. The amounts of the drug released were determined based on the previously constructed calibration curve by measuring the absorbance every 5 s until the complete dissolution of the fibrous samples. The dissolution was conducted in triplicate, and the nepafenac release curve was built from the average value of the three measurements. The kinetics of the nepafenac release from nanofibers were then evaluated using Weibull model based on the Equation (3):

$$M_t = M_\infty \left(1 - e^{-\frac{(t-t_0)^\beta}{\tau_d}}\right) \quad (3)$$

where M_t is the nepafenac release at (t) time, while M_∞ is the maximum amount of the released nepafenac. The parameters t_0 and τ_d are the lag time and average dissolution time, respectively. The shape of the release curve is specified by the β parameter ($\beta = 1$ denotes first-order kinetics, $\beta > 1$ indicates a slow onset followed by an accelerated release, and $\beta < 1$ indicates a fast onset followed by a slow release) (Kazsoki et al., 2022; Pourtalebi Jahromi et al., 2020).

2.2.8. Permeability studies

2.2.8.1. In vitro corneal-PAMPA assay. Right before the experiment, electrospun samples were dissolved in PBS to create solutions with 1 mg/ml concentration, then the samples were diluted 20-fold to mimic tear production. Nevanac® (1 mg/mL) was diluted 20-fold with PBS. In the case of the test formulations, each matching well of the acceptor plate (Multiscreen Acceptor Plate, MSSACCEPTOR; Millipore) were

filled with HPßCD solution to reduce the reverse sink effect (containing 10 % HPßCD of the diluted electrospun-samples) whereas in the case of Nevanac® the acceptor wells were filled with PBS. Each sample were measured in six replicates. The artificial membrane was fabricated by dissolving 16 mg phosphatidylcholine in a solvent mixture of dodecane, hexane and chloroform (25:70:5 v/v) and coating each well of the donor plate (MultiscreenTM-IP, MAIPN4510, pore size 0.45 mm; Millipore) with 5 µL of the lipid solution (Dargó et al., 2019).After that, the donor plate was filled with 150 µL sample solutions. Finally, the sandwich plate was assembled and covered with a wet sheet of paper and a plate lid to avoid evaporation. The system was incubated for 4 h at 35 °C (Heidolph Titramax 1000, Heidolph Instruments, Swabach, Germany). After that, initial, donor and acceptor samples were collected and analysed by HPLC-DAD. Effective permeability was calculated using the Eqs. (4) and (5):

$$P_e = \frac{-2.303}{A \bullet (t - \tau_{ss})} \bullet \left(\frac{1}{1 + r_v}\right) \bullet \lg\left[-r_v + \left(\frac{1 + r_v}{1 - MR}\right) \bullet \frac{c_D(t)}{c_D(0)}\right] \quad (4)$$

$$MR = 1 - \frac{c_D(t)}{c_D(0)} - \frac{V_A c_A(t)}{V_D c_D(0)} \quad (5)$$

where A is the filter area (0.3 cm^2), V_D and V_A are the volumes in the donor (0.15 cm^3) and acceptor phase (0.3 cm^3), *t* is the incubation time (s), τ_{SS} is the time to reach steady-state (s), $c_D(t)$ is the concentration of the compound in the donor phase at time point t (mol/cm^3), $c_D(0)$ is the concentration of the compound in the donor phase at time point zero (mol/cm^3), $c_A(t)$ is the concentration of the compound in the acceptor phase at time point t (mol/cm^3), r_v is the aqueous compartment volume ratio (V_D/V_A). For the comparison, the same experiment was repeated with omitting the effect of HPβCD.

2.2.8.2. Ex vivo corneal permeability studies on porcine eyes. For the ex vivo assay, electrospun samples were dissolved in PSS right before the experiment. Freshly donated porcine eyes obtained from the slaughterhouse were placed on a sterile cotton wool bed moistened with physiological saline solution and kept in a refrigerator box during transportation. The porcine eyes were first placed into PTFE inserts, where the cornea was uncovered and surrounded by a PTFE ring to prevent the flow of eye drops (Vincze et al., 2023). The orifice above the corneal surface was first washed with PSS, and then the devices were pre-incubated at 35 °C in a water bath for 5 min. After that, PSS was removed from the corneal surface, and 100 µL of the undiluted formulations were pipetted on each cornea using 3 eyes for each formulation, then the devices were incubated for 1 min. After that, the samples on the eye surface were diluted by adding PSS to the device's orifice to reach a 20-fold diluted concentration of the original dose (~0.05 mg/mL), and the eyes were incubated with these diluted formulations for another 14, 29, or 59 min. At these endpoints, diluted formulations were removed from the precorneal area, the devices were disassembled, then aqueous humor was drained using a 26G needle, and finally the cornea was excised and NEP was extracted with 2 mL of AcN:water 50:50 (v/v) using an orbital shaker (Heidolph Titramax 100, Heidolph Instruments, Swabach, Germany) for 60 min at 450 rpm. Samples of precorneal fluid, aqueous humor, and corneal extract were analyzed by HPLC-DAD, and the nepafenac concentration was calculated using a calibration curve. The corneal retention (CR) of nepafenac, the apparent permeability ($P_{app}C$) of nepafenac into the cornea, and the apparent permeability ($P_{app}Aq$) of nepafenac into the aqueous humor were calculated using Equations (6)–(8), respectively.

$$CR = 1 - \frac{c_{CS}(t)}{c_{CS}(0)} - \frac{V_{AC} c_C(t)}{V_{CS} c_{CS}(0)} \quad (6)$$

$$P_{app}C(cm/s) = \frac{\Delta[C]_C \times V_{AC}}{A \times [C]_{CS} \times \Delta t} \quad (7)$$

$$P_{app}Aq(cm/s) = \frac{\Delta[C]_{Aq} \times V_{AC}}{A \times [C]_{CS} \times \Delta t} \quad (8)$$

where $c_{CS}(t)$ is the concentration of the compound on the corneal surface at time point *t* (mol/cm^3), $c_{CS}(0)$ is the concentration of the compound on the corneal surface at time point zero (mol/cm^3), $c_C(t)$ is the concentration of the compound in the cornea at time point *t* (mol/cm^3), and V_{AC} and V_{CS} are the volumes in the anterior chamber (0.25 cm^3) and on the corneal surface (0.75 cm^3).

$P_{app}C$ was calculated from the concentration difference of NEP in the aqueous humor ($\Delta[C]_C$) after treatment, the initial concentration of the compound on the corneal surface at time point zero ($c_{CS}(0)$), the volume on the corneal surface V_{CS} (0.75 cm^3), *A* is the surface area available for permeability (1.77 cm^2), and *t* is the incubation time (s). $P_{app}Aq$ was calculated from the concentration difference of NEP in the cornea ($\Delta[C]_{Aq}$) after treatment, the initial concentration of the compound on the corneal surface at time point zero ($c_{CS}(0)$), the volume on the corneal surface V_{CS} (0.75 cm^3), *A* is the surface area available for permeability (1.77 cm^2), and *t* is the incubation time (s).

2.2.8.3. Ex vivo cornea Raman mapping. Parallel with the corneal permeability determined with HPLC, the distribution of NEP (nepafenac) in the excised cornea was also investigated with Raman mapping after 15-, 30-, and 60-minute treatment. The cornea was frozen after the treatment and divided into cross sections (15 µm thick) with a Leica CM1950 Cryostat (Leica Biosystems GmbH, Wetzlar, Germany). The selected specimens were mounted on aluminum-coated slides before the experiment. Raman spectroscopic analysis was performed with a Thermo Fisher DXR Dispersive Raman Spectrometer (Thermo Fisher Scientific Inc., Waltham, MA, USA) equipped with a CCD camera and a diode laser with a wavelength of 780 nm. For marking the corneal area for investigation, an objective with 50x magnification was used. For the measurements, a laser power of 24 mW was used, and a slit aperture with a 50 µm size was applied. Raman maps were captured from an area of 150 × 1000 µm, with a step size of 50 µm vertically and horizontally. The OMNIC for Dispersive Raman 8.2 software (Thermo Fisher Scientific) was used for chemical evaluation. The individual spectrum of unformulated NEP was used as a reference when profiling the chemical map.

2.2.9. Hen's egg test on chorioallantoic membrane (HET-CAM)

The HET-CAM test was performed to evaluate the biocompatibility of the developed formulations by observing if hyperemia, hemorrhage, and coagulation were induced after direct application of the ocular films on the chorioallantoic membrane (CAM) of 9-day-old chicken embryos. The test has been conducted based on the reported work (Luepke, 1985). Fertilized White Leghorn chicken (*Gallus gallus domesticus*) eggs were obtained from commercial breeders (Prophyl-BIOVO Hungary Ltd., Mohacs) and maintained at a temperature of 37.5 °C ± 0.5 °C in a humidified HEKA 1 + egg incubator (Rietberg, Germany). On the 9th day of incubation, a small hole was created using fine forceps at the blunt end of the eggs, then the hole on the hard eggshell was expanded to about 2 cm with ophthalmic surgical scissors, followed by careful removal of the inner membrane to expose the vascularized CAM. On the surface of the vascularized CAM, plain and nepafenac-loaded nanofiber mats were placed and evaluated against phosphate-buffered saline (PBS) pH 7.4 and 0.1 N NaOH solution as negative and positive controls, respectively. After 20 s of applying the tested materials, the vascular CAM was irrigated with 5 mL of PBS and evaluated for irritation effects. Images were captured at 0.5, 2, and 5 min using a Nikon SMZ25 stereomicroscope (Unicam Ltd., Hungary). Image processing was conducted using Nikon's proprietary software, QCapture Pro. Each sample was given a score based on the numerical time-dependent scores for hyperemia, hemorrhage, and coagulation (Andreadis et al., 2022; Luepke, 1985).

2.2.10. Accelerated stability study

For the accelerated stability study, the nepafenac-loaded electrospun samples were collected in aluminum foils and packed into hermetic bags with zip closures. The samples were stored in a stability chamber (Sanyo type 022, Leicestershire, UK) for 4 weeks under controlled conditions (40 ± 2 °C, 75 ± 5 % relative humidity). The samples were subjected to SEM and FTIR evaluations in 0, 1, 2, 3, and 4 weeks to study the effect of applying elevated levels of temperature, humidity, and pressure on the morphology and solid-state characters of the NEPA-loaded electrospun nanofibers.

2.2.11. Statistical analysis

The statistical analysis and figures were prepared using OriginPro 2018 software (v9.5.1., OriginLab Corporation, Northampton, MA, USA). ANOVA tests were used to assess the difference between the data. A p-value of less than 0.05 was considered statistically significant. For assessing the normality of fiber diameters distribution, skewness and curtosis have been calculated by using Microsoft Excel 2010 functions.

3. Results and discussion

3.1. Solution of NEPA/ HPβCD in water

The solution of nepafenac in water has been prepared based on a published work (Lorenzo-Veiga et al., 2019), and it has been confirmed that each 1 mg/mL (3.9 mM) of nepafenac can be dissolved by adding approximately 0.069 g (50 mM) of HPβCD to produce a clear yellow solution. The amount of the dissolved nepafenac was successfully determined and confirmed according to a previously constructed calibration curve.

3.2. Morphological evaluation

The morphological features of the electrospun samples were studied using a scanning electron microscope (SEM). The SEM images and corresponding fiber diameter distributions are displayed in Figs. 1 and 2, respectively.

The images show bead-free, randomly oriented fiber depositions and no gel droplets on the fibers' surfaces, with fiber diameters ranging from 124 ± 20 nm to 464 ± 49 nm. The results reflect that the selected polymers (PVA/Poloxamer 407) and the drug complex (NEPA/HPβCD) are appropriate for fiber formation within the designated drug-to-polymer ratios. It has been observed that increasing the HPβCD amount results in a better fiber's surface with more clear, smoother, and more uniform fibers. This enhancement in the fiber structure might be attributed to the unique physicochemical properties of HPβCD and its ability to form self-assembling aggregates that enhance the intermolecular interactions of the components of the electrospinning solution (Dodero et al., 2021).

Although there was no significant difference between average fiber

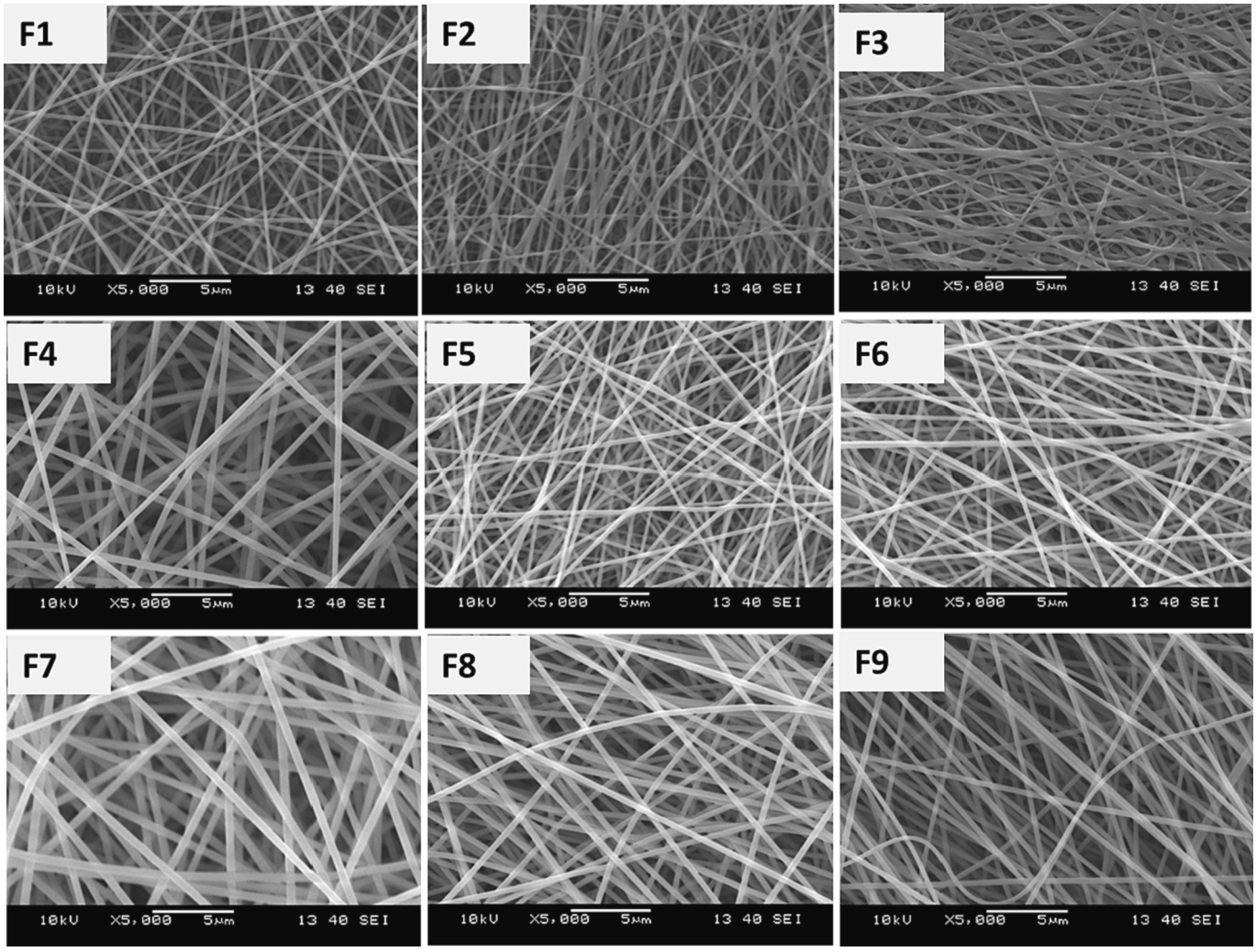

Fig. 1. Scanning Electron Microscope (SEM) images of Nepafenac-loaded electrospun samples prepared from nepafenac/ hydroxypropyl-beta-cyclodextrin/polyvinyl alcohol (NEPA/HPβCD/PVA) (F1, F4, and F7); and NEPA/ HPβCD/PVA/Poloxamer 407 (F2, F3, F5, F6, F8, and F9) (magnification: 5000×).

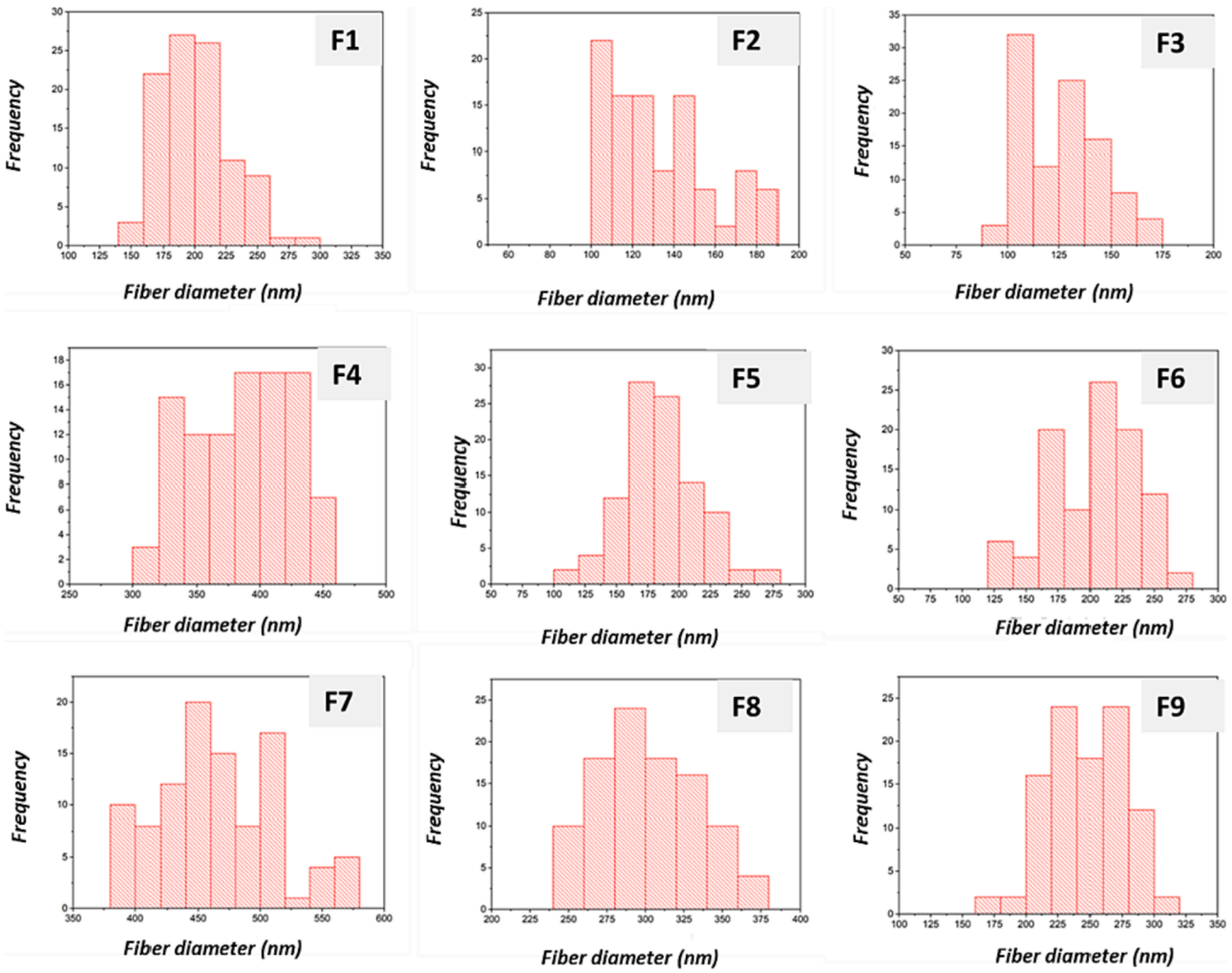

Fig. 2. Fiber diameter distributions of Nepafenac-loaded electrospun samples prepared from nepafenac/ hydroxypropyl-beta-cyclodextrin/polyvinyl alcohol (NEPA/ HPβCD/PVA) (F1, F4, and F7); and NEPA/ HPβCD/PVA/Poloxamer 407 (F2, F3, F5, F6, F8, and F9).

diameters at p-value < 0.05 ($p = 0.16921$), the histograms showed different diameter distributions (Fig. 2). The presence of HPβCD in low amounts (F2 and F3) resulted in a lower average fiber diameter when compared to the double and triple the amount in the formulations (F5 and F6) and (F8 and F9), respectively. This effect can be attributed to the increased solution viscosity (Haider et al., 2018) and/or the presence of HPβCD in higher amounts. The latter may interfere with the surface active effect of poloxamer 407 (thinning effect) and increase the solution entanglement and intermolecular interactions (Dodero et al., 2021; Haider et al., 2018).

3.3. Effect of poloxamer 407 and HPβCD on the diameter distribution

Based on the morphological results, there is great diversity among different formulations. The calculated average fiber diameters, skewness, and kurtosis values are shown in Table S1. Most formulations containing HPβCD have skewness values within an acceptable range, and the distribution curves are symmetric (the absolute skewness values lie between −0.5 and + 0.5). The exceptions are F1 and F2, which showed moderate skewness values lying between + 0.5 and + 1. Results revealed no definite relationship between HPβCD content and histograms or skewness values. The fiber distribution curves showed variable behavior (Figure S1). This ununified behavior can be justified by the fact that electrospun nanofibers are not only evaluated by the SEM images, but further analyses to be conducted to evaluate and characterize normally distributed curves from compound distribution curves. This fiber's behavior proves that many factors overlap during electrospinning including, for instance, the precursor solution composition as well as the process parameters. The kurtosis values for the fiber distribution showed no very sharp peak or too flat curve (k values between + 1 and −1). Some formulations showed good fit ($R^2 \geq 0.95$) to the normal distribution, while the rest did not fit. These results are in accordance with skewness calculations (distribution curves are of symmetric and moderately skewness types).

3.4. FTIR analysis

FTIR analysis was conducted to study the structural changes in the components of NEPA-loaded electrospun nanofibers. The spectra of all individual components, including NEPA, PVA, poloxamer 407, and HPβCD and the spectra of electrospun fibrous samples are presented in Fig. 3. The spectra of nepafenac powder showed the following distinctive peaks: medium absorption bands at 3317.92 cm^{-1} and 3326.6 cm^{-1} confirmed N-H_2 stretching; a peak appeared at 1676 cm^{-1} is attributed to C = C stretching; N–H bending appeared at 1554 cm^{-1}; a peak at1283 cm^{-1} is attributed to stretching of aromatic amine; an absorption peak at 1236 cm^{-1} is due to stretching of aliphatic amine (Lorenzo-Veiga et al., 2019; Mecozzi & Sturchio, 2017; Shelley et al., 2018).

The spectra of HPβCD showed the most important peaks as follows: a broad band at 3200 cm^{-1}–3485 cm^{-1} characteristic of O–H stretching

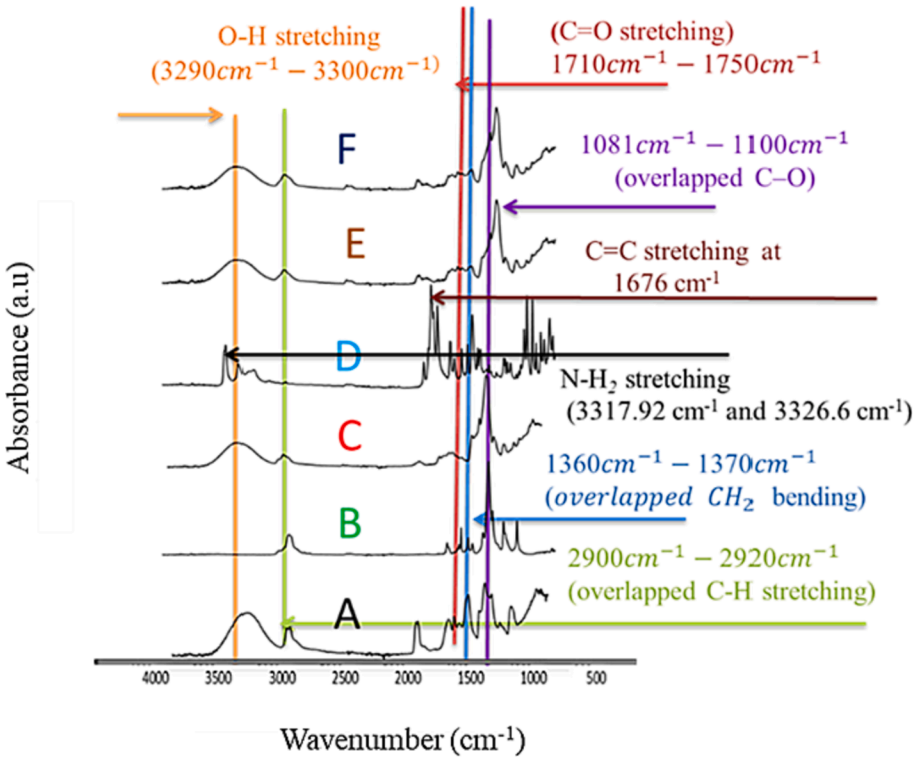

Fig. 3. Fourier transform infrared (FTIR) spectra of: (A): polyvinyl alcohol (PVA) (physical form); (B): Poloxamer 407 (physical form); (C): Hydroxypropyl-β-cyclodextrin (HPβCD); (D): Nepafenac (NEPA) (physical form); (E): Electrospun nanofibers of NEPA/HPβCD/PVA (F1, F4, and F7); and (F): Electrospun nanofibers of NEPA/ HPβCD/PVA/Poloxamer 407 (F2, F3, F5, F6, F8, and F9). The PVA grade used was intermediate molecular weight (Mw ~ 130 kDa).

arising from the intermolecular and intra-molecular hydrogen bonds; an absorption band at 2912 cm^{-1}–2986 cm^{-1} characteristic of C–H stretching; a peak at 1670 cm^{-1} is attributed to C = C stretching; a strong, sharp peak at 1024.9 cm^{-1} is related to C-O stretching (Mecozzi & Sturchio, 2017; Topal et al., 2015).

The PVA spectra showed the following important peaks: a broad band at 3282 cm^{-1}–3300 cm^{-1}characteristic for O–H stretching arising from the intermolecular and intra-molecular hydrogen bonds; the band at 2910 cm^{-1}–2920 $cm^{-1}$is related to C–H stretching from alkyl group; the band at 1710 cm^{-1}–1750 cm^{-1} is attributed to carbonyl (C = O stretching); the band at 1400 cm^{-1}–1420 cm^{-1} is due to bending stretching of CH_2; the band at 1345 cm^{-1}–1370 cm^{-1} resulting from C-H vibration; the band at 1080 cm^{-1}–1090 cm^{-1} is related to C-O stretching of acetyl groups; and the band at 830 cm^{-1}–840 cm^{-1} is attributed to C–C stretching vibration (Bhat et al., 2005; García-Millán et al., 2017; Kharazmi et al., 2015; Mansur et al., 2008).

Regarding poloxamer 407 spectra, the absorption peak at 2939 cm^{-1} is related to CH_3 stretching; the peak at 2872 cm^{-1} is due to CH_2 stretching; absorption bands at 1095 cm^{-1} and 1340 cm^{-1} are attributed to C-O stretching and O–H bending, respectively (Ellakwa et al., 2017; Laurano et al., 2020; Yasser et al., 2019). The spectra of the nanofiber blends (PVA/poloxamer 407/nepafenac/HPβCD) display the presence of the main distinctive peaks of PVA, Poloxamer 407, and HPβCD: An overlapped absorption band ranging at 3118.3 cm^{-1}–3598.5 cm^{-1} (overlapped band of N-H_2 stretching from nepafenac and O–H stretching from PVA and HPβCD); an overlapped absorption peak at 2823.2 cm^{-1}–2995.8 cm^{-1} (overlapped band of C–H stretching from PVA, Poloxamer 407 and HPβCD); absorption band at 1704 cm^{-1}–1744 cm^{-1} related to carbonyl (C = O stretching of PVA); an overlapped absorption band appeared at 1670 cm^{-1}–1674 cm^{-1} (is attributed to C = C stretching); absorption peak at 1360 cm^{-1}–1370 cm^{-1} indicating overlapped CH_2 bending stretching from PVA and O–H bending from poloxamer 407; a strong sharp peak at 1024.9 cm^{-1} is related to that arising from C-O stretching of HPβCD; absorption peak at 1081 cm^{-1}–1100 cm^{-1} indicating overlapped peak due to C–O stretching from (PVA, poloxamer 407); and peak at 828 cm^{-1}– 840 cm^{-1} is related to C–C stretching vibration of PVA. The O–H absorption of nanofibers blends (PVA/poloxamer 407/nepafenac/HPβCD) was lower than that of individual PVA and HPβCD. This may be due to the incorporation of nepafenac into HPβCD via inclusion complex and interaction of the resulting complex with O–H of the PVA.

3.4.1. X-ray diffraction (XRD)

The R-ray diffraction patterns of the NEPA, physical mixture, F3, F6, and F9 are displayed in Figure S3. The presence of sharp peaks confirmed the crystallinity of the NEPA in its pure state. The intensities of the peaks have decreased upon mixing the NEPA with HPCD, PVA, or polymer 407. The complete disappearance of these peaks from the nanofibers (F3, F6, and F9) confirms the formation of amorphous solid dispersion from crystalline nepafenac through electrospinning of NEPA, HPβCD, PVA, and Poloxamer 407.

3.5. Determination of the drug content

The drug content of all formulations (F1–F9) of nepafenac-loaded nanofibers ranged from 100.01 (% w/w) ± 0.03 to 101.05 (% w/w) ± 0.02. The results show uniform drug content throughout the PVA/poloxamer 407 fiber structure. This reflects the complete dissolution of the nepafenac through complexation with HPβCD during the solution preparation. During electrospinning, a homogenous precipitation of the drug/polymer blend occurred after solvent evaporation. Therefore, any deviation from the theoretically stated amounts might be attributed to errors that can occur during solution preparation or during fibers' weighing.

3.6. In vitro drug release and release kinetics

In vitro dissolution profiles of the NEPA/ HPβCD-loaded nanofibers

(0.1 % w/w) conducted in phosphate buffered solution (pH 7.4) at 37 °C are displayed in Fig. 4. All formulations (F1-F9) showed complete release of nepafenac in less than 60 min (16.5—40 min). The fast release of the drug from nanofibers can be explained by the formation of amorphous solid dispersion. All formulations completely dissolved within 5 s, forming a viscous gel when placed on the surface of filter paper wetted with a phosphate buffered solution (pH 7.4), as shown in Table S2, which are in good agreement with the previously published work (Pandit et al., 2023). Regardless of HPβCD amount, all formulations containing poloxamer 407 (F2, F3, F5, F6, F8, and F9) released the nepafenac at a faster rate compared to the formulations without poloxamer 407. This can be attributed to the surface-active effects of poloxamer 407, resulting in faster disintegration and dissolution of the formulations. Some variations were observed in the dissolution profiles with varying the HPβCD and poloxamer 407 amounts. Higher HPβCD levels resulted in a longer drug release, while higher poloxamer 407 levels resulted in a faster release ($p = 0.03253$ at p-value < 0.05). In a conclusion, there was no significant difference in the overall release of the nine formulations. Since each drug-loaded fiber formulation is within the nanometer scale, it is straightforward that there is no great difference in the surface and the consequent release among the different formulations. Therefore, factors other than the diameter of the fibers were considered. The formulations F3, F6, and F9 (with different ratios of HPβCD) were chosen for further permeability studies. Based on published works HPβCD resulted in enhancing the ophthalmic permeability of dexamethasone from hydrogel system (Kesavan et al., 2011), and in some cases, it can decrease permeability (Loftsson et al., 2007).

The release kinetics of nepafenac from nanofibrous matrix was studied using Weibull distribution due to the flexibility of the model in dealing with diverse release patterns. The release parameters including M_∞, β, τ_d and R^2 are summarized in Table 2. All formulations (F1-F9) were successfully fitted to the Weibull model and R^2 values were greater than 0.9 indicating linear regression. The shape of the release curve was found to follow first-order release (β values for all formulation were < 1) with good correlation.

Table 2
Dissolution kinetic parameters of Nepafenac (NEPA) (0.1%w/w)/Hydroxypropyl-β-cyclodextrin (HPβCD) loaded in polyvinyl alcohol/poloxamer 407 nanofibers.

Formulation code	M_∞ (min)	β Parameter	τ_d (min)	Correlation Coefficient (R^2)
F1	100.3	0.6838	128.7	0.9929
F2	102.3	0.5154	121.4	0.9858
F3	100.4	0.8466	105.7	0.9909
F4	99.0	0.6501	88.4	0.9896
F5	103.5	0.4222	110.3	0.9824
F6	100.1	0.5807	92.7	0.9751
F7	96.2	0.8506	103.3	0.9681
F8	119.2	0.2479	259.1	0.9397
F9	98.6	0.9268	104.9	0.9812

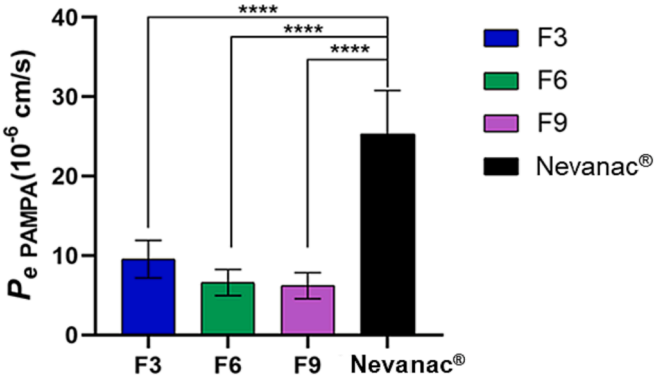

Fig. 5. In vitro Corneal-PAMPA studies for the formulation F3, F6 and F9. Using nepafenac commercial product Nevanac®).

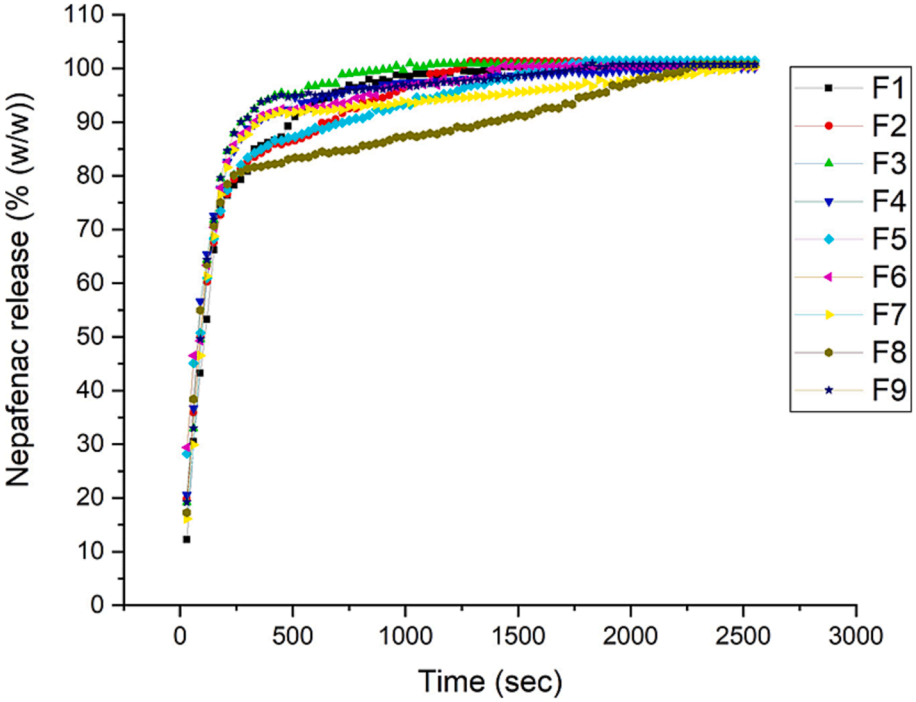

Fig. 4. In vitro dissolution profiles of Nepafenac (NEPA)/ Hydroxypropyl-β-cyclodextrin (HPβCD) (0.1 %w/w) loaded in polyvinyl alcohol (PVA)/poloxamer 407 nanofibers. The dissolution was conducted in phosphate buffered solution (pH 7.4) at 37 °C.

3.7. Permeability studies

3.7.1. In vitro corneal-PAMPA assay

PAMPA permeability assay results are presented in Fig. 5. Results from experiment showed no significant difference between the 3 formulations (F3, F6 and F9) regardless of the HPβCD content per formulation (50 mM, 100 mM and 150 mM for F3, F6 and F9 respectively). However, their permeability values were significantly lower than the value measured for Nevanac® ($p < 0.05$). In the case of the PAMPA system where only passive diffusion occurs through the artificially fabricated lipid membrane, a reverse sink is created as the donor compartment contains HPβCD (in high amount) as solubilizing agent. To mitigate this reverse sink effect, 10 % of the donor's HPßCD content was added to the acceptor wells to create a more desirable environment for the poorly soluble nepafenac molecules. Unfortunately, in this case corneal-PAMPA could not make a difference between the three formulations. The experiments conducted using PBS acceptor media resulted different tendencies within the samples containing various amounts of HPβCD. The increase in HPβCD amount among the 3 formulations resulted in an increased flux of nepafenac to the acceptor compartment. The average permeabilities ± SD (10–6/cm) for the F3, F6, and F9 formulations were 11.9 ± 2.21, 13.8 ± 1.59, and 21.6 ± 2.968 respectively. However, F3 is a good choice as it contains the least amount of CD and shows similar average permeability values independently the applied models. The lower amount of CD can be physiologically favorable for the penetration process (Loftsson et al., 2007). Therefore, F3 was chosen for the ex vivo study. Moreover, conducting the experiment in only phosphate-buffered media, omitting the reverse sink effect of HPβCD, the same permeability value was obtained in the case of F3.

3.7.2. Ex vivo corneal permeability studies on porcine eyes

The concentration of the NEPA for the F3 in precorneal area, cornea, and aqueous humor has been determined at 15, 30, and 60 min. The results of Fig. 6 show that F3 has a significantly higher concentration than Nevanac® in precorneal area, and this can be attributed to the complete dissolution of the NEPA-loaded nanofibers, as shown in Fig. 6A. The values for the concentrations of nepafenac in precorneal fluid for F3 and commercial Nevanac®at 15, 30 and 60 min were found to be 0.0269, 0.0013 and < 0.0001 respectively. The highest dissolution was attained at 60 min, which means the F3 had sufficient time to release more NEPA from the formulation. Regarding the cornea, although there is a slight increase in the Nevanac® compared to F3 formulation, it is only a numerical difference without statistical significance (Fig. 6B). The NEPA concentrations in the aqueous humor were not significantly different at 15 and 30 min (Fig. 6C). At 60 min Nevanac® had a significantly higher concentration than F3 formulation, with *p value* at 0.05 level of confidence being 0.0242. By compiling all these findings, it can be concluded that bioequivalent drug concentrations might be obtained if the study is conducted in vivo.

3.7.3. Ex vivo cornea Raman mapping

The NEPA distribution within corneal tissues has been studied using Raman mapping. The F3 exposed porcine corneal tissues are presented in Fig. 7. Based on the intensity scale, the high concentration of NEPA is reflected by the red color, the green color reflects lower concentration, whereas the blue color represents the area of the map where spectral resolution specify the untreated corneal tissue. The results show that in both cases NEPA distribution at 15 min was restricted to outer layers of the cornea, but it distributed to the inner most layer (stroma) at 30 and 60 min with more homogenous feature. In conclusion, there results support our finding that F3 could be bioequivalent to Nevanac® in vivo.

3.8. Hen's egg test on chorioallantoic membrane (HET-CAM)

All applied samples, including plain fibers, nepafenac-loaded fibers, and negative controls, have not resulted in any noticeable irritation on the CAM surface when compared to the positive control (0.1 N NaCl). The results suggest the cytocompatibility of the formulation components. The HET-CAM results are displayed in Fig. 8. These results confirm that the ingredients of the formulation are well tolerated. Despite its simplicity, the HET-CAM method can be utilized as a surrogate for the Draize test. The increasing research in ocular formulations dictates less animal-intensive experimental methods; therefore, a method that mimics the in vivo Draize test should be a valid alternative to comply with the global 3R's requirements. This test falls on the borderline between in vitro and in vivo, which means reduction and/or elimination of pain and injuries when performing the experiments on whole animals, in addition to the accurate results demonstrated by this model.

3.9. Accelerated stability study

The scanning electron microscope images of the nepafenac-loaded electrospun nanofibers for the freshly prepared samples and samples stored under stressful conditions are illustrated in Fig. 9. It can be observed that samples retained their morphological features despite exposure to elevated levels of temperature, humidity, and pressure. Stability under these stressful conditions could be taken to indicate the long-term stability under ambient conditions. The fibrous structures have been maintained throughout the whole period of study (4 weeks). No considerable morphological changes were observed, and the sample remained fibrous during the whole period of study.

The time dependent changes in physicochemical characteristics of the Nepafenac-loaded nanofibers exposed to stressful conditions have

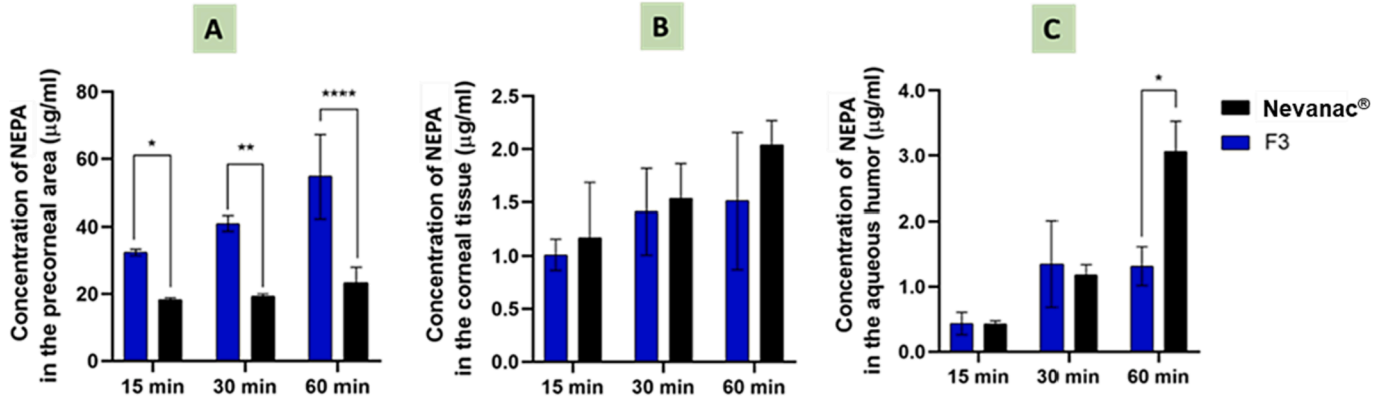

Fig. 6. Nepafenac concentration of F3 for ex vivo experiment on porcine eye measured at (A): precorneal area; (B): cornea; and (C): aqueous humor, using Nevanac® as reference.

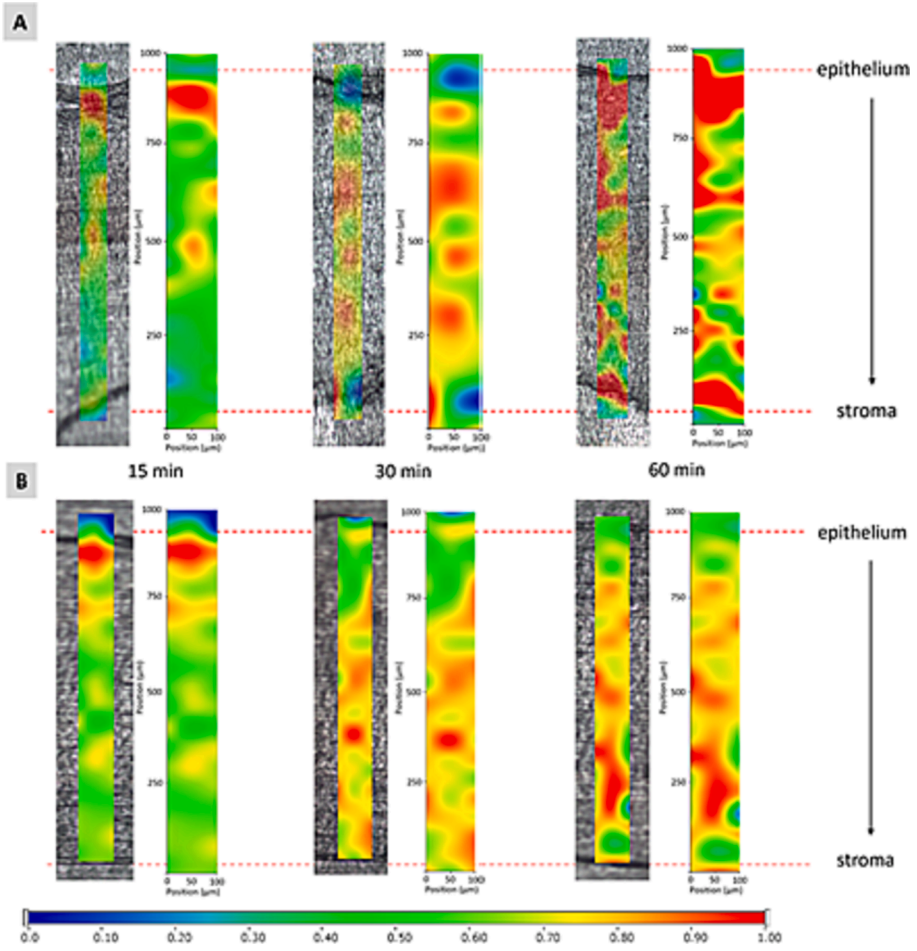

Fig. 7. The Raman mapping of the distribution nepafenac in the excised porcine cornea for F3 formulation (A) and Nevanac® (B). The high concentration of NEPA is reflected by the red color, the green color reflects lower concentration, whereas the blue color represents the area of the map where spectral resolution specify the untreated corneal tissue. (For interpretation of the references to color in this figure legend, the reader is referred to the web version of this article.)

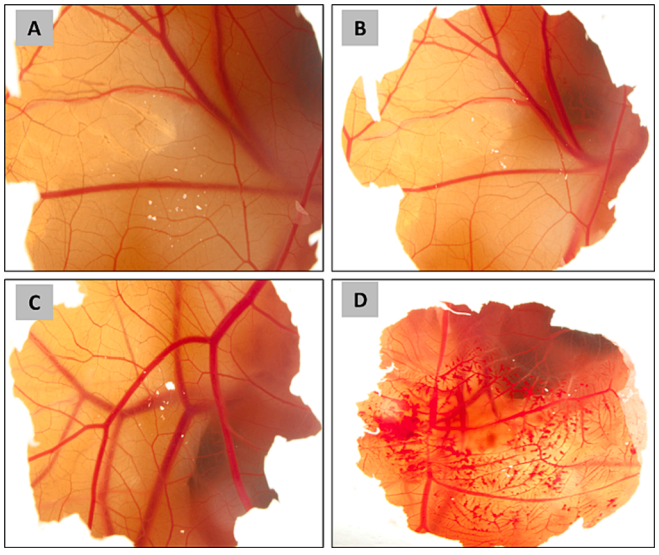

Fig. 8. Representative images of Hen's Egg Test on Chorioallantoic Membrane (HET-CAM) conducted for a period of 5 min. (A): PBS (negative control); (B): Empty fibers polyvinyl alcohol (PVA)/ Hydroxypropyl-β-cyclodextrin (HPβCD)/ poloxamer 407; (C): Nepafenac-loaded fibers; (D): 0.1 N NaOH (positive control).

been displayed in Fig. 10. Elevated temperature and humidity have no substantial effects on the essential functional groups of the fibrous samples during the period of study. These results come along with morphological studies. In conclusion, this short-term stability test under stressful conditions suggests that a stable, solid nanofibrous formulation could be successfully obtained using preservative-free components.

4. Conclusion

Nanofibrous webs can be utilized as potential candidates regarding novel technologies for targeting ophthalmic diseases. Because of their advantages compared to conventional topical formulations, they can deliver myriad number of drugs including water soluble, water insoluble, genes and proteins as well as agents for corneal regeneration and cell proliferation. On the other hand, it can be a suitable candidate to overcome the inherited ocular barriers including anatomical, physiological as well as biochemistry barriers. Therefore, it can be considered as a smart platform for current and future issues. The HPβCD not only improved the solubility of NEPA through inclusion complex formation, but also enhanced the spinnability of the precursor solution. SEM results showed that smooth fibers can be obtained. FTIR spectra confirmed the compatibility of the matrix formers with the active. Formation of amorphous solid dispersion was confirmed by FTIR spectra and XRD analysis. The release and in vitro kinetics studies showed immediate release of the drug, which was characterized by the model-independent Weibull distribution. The porous feature of nanofiber webs, along with their high surface-to-volume ratio, resulted in rapid dissolution of the

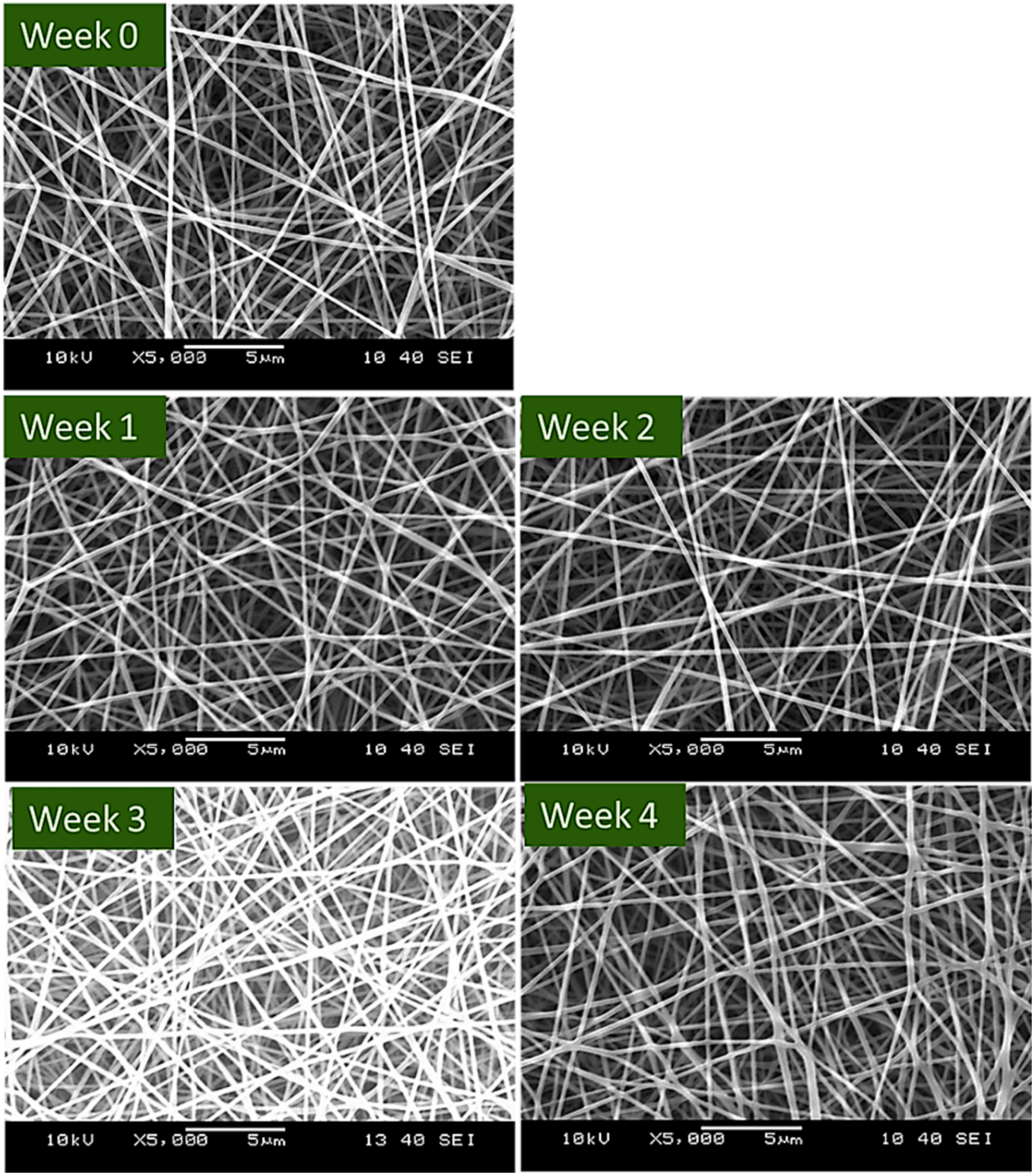

Fig. 9. Scanning electron microscopic (SEM) images of the Nepafenac-loaded fibers at 0, 1, 2, 3, and 4 weeks storage under stress conditions (40 ± 2 ∘C, 75 ± 5 % relative humidity). (magnification: 5000×).

proposed ophthalmic inserts upon contact with the phosphate buffer solution. The permeability results showed a good penetration of the developed formulation to the corneal layers and the component of the developed polymeric matrix displayed a good compatibility with HET_CAM of fertilized chicken embryos. In conclusion, the obtained results reflect that the electrospun NEPA-loaded nanofibers-based ocular inserts could be a promising alternative to conventional systems with better bioavailability and stability.

Funding

This project was supported by New National Excellence Program of the Ministry for Culture and Innovation from the source of the National Research, Development, and Innovation Fund (ÚNKP-22-3-II-SE-78 and

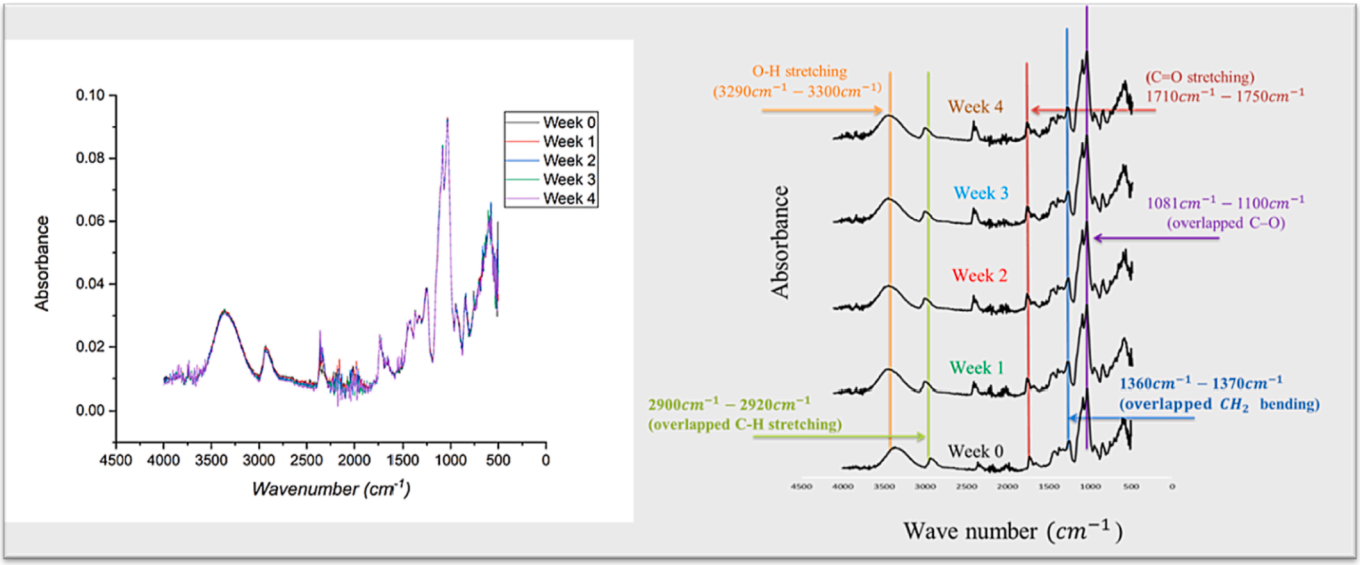

Fig. 10. Fourier transform infrared (FTIR) spectra of the Nepafenac-loaded fibers at 0, 1, 2, 3, and 4 weeks storage under stress conditions (40 ± 2 ∘C, 75 ± 5 % relative humidity).

ÚNKP-22-4-II-SE-29), Central Europe Leuven Strategic Alliance (CELSA-2021/019) and, by an FK-137582 grant from the National Research and Innovation Office, Hungary (NRDI).

CRediT authorship contribution statement

Safaa Omer: Conceptualization, Methodology, Formal analysis, Investigation, Data curation, Writing – original draft. **Nándor Nagy:** Methodology, Investigation, Writing – review & editing. **Emőke Szőcs:** Methodology, Investigation. **Szabina Kádár:** Methodology, Formal analysis, Investigation. **Gergely Völgyi:** Methodology, Formal analysis, Investigation. **Balázs Pinke:** Investigation, Visualization. **László Mészáros:** Investigation, Visualization. **Gábor Katona:** Methodology, Formal analysis, Investigation. **Anna Vincze:** Methodology, Formal analysis, Investigation. **Péter Dormán:** Methodology, Investigation. **Zoltán Zs. Nagy:** Methodology. **György T. Balogh:** Methodology, Formal analysis, Investigation, Writing – review & editing. **Adrienn Kazsoki:** Writing – review & editing, Supervision. **Romána Zelkó:** Writing – review & editing, Supervision.

Declaration of Competing Interest

The authors declare that they have no known competing financial interests or personal relationships that could have appeared to influence the work reported in this paper.

Data availability

Data will be made available on request.

Acknowledgments

The authors would like to thank Maria Budai-Szűcs from University of Szeged for her help in the preparation of treated corneal tissue for Raman investigation, and Bence Tóth for his help in x-ray diffraction analysis.

Appendix A. Supplementary material

Supplementary data to this article can be found online at https://doi.org/10.1016/j.ijpharm.2023.123554.

References

Aleo, D., Saita, M.G., Spitaleri, F., Sanfilippo, C., Patti, A., 2020. Degradation profile of nepafenac in aqueous solution and structural characterization of a novel degradation product. J. Pharm. Biomed. Anal. 189, 113432 https://doi.org/10.1016/j.jpba.2020.113432.

Andreadis, I.I., Karavasili, C., Thomas, A., Komnenou, A., Tzimtzimis, M., Tzetzis, D., Andreadis, D., Bouropoulos, N., Fatouros, D.G., 2022. In Situ Gelling Electrospun Ocular Films Sustain the Intraocular Pressure-Lowering Effect of Timolol Maleate. In Vitro, Ex Vivo, and Pharmacodynamic Assessment. Mol. Pharm. 19 (1), 274–286. https://doi.org/10.1021/acs.molpharmaceut.1c00766.

Barse, R.K., Tagalpallewar, A.A., Kokare, C.R., Sharma, J.P., Sharma, P.K., 2017. Formulation and ex vivo- in vivo evaluation of pH triggered brimonidine tartrate in situ gel for the glaucoma treatment using application of 32 factorial design. Drug Dev. Ind. Pharm. 000. https://doi.org/10.1080/03639045.2017.1414229.

Bhat, N.V., Nate, M.M., Kurup, M.B., Bambole, V.A., Sabharwal, S., 2005. Effect of γ-radiation on the structure and morphology of polyvinyl alcohol films. Nucl. Instrum. Methods Phys. Res., Sect. B 237 (3–4), 585–592. https://doi.org/10.1016/j.nimb.2005.04.058.

Chen, H., Jin, Y., Sun, L., Li, X., Nan, K., Liu, H., Zheng, Q., Wang, B., 2018. Recent Developments in Ophthalmic Drug Delivery Systems for Therapy of Both Anterior and Posterior Segment Diseases. Colloids Interface Sci. Commun. 24 (April), 54–61. https://doi.org/10.1016/j.colcom.2018.03.008.

Dargó, G., Vincze, A., Müller, J., Kiss, H.J., Zsolt, Z., 2019. European Journal of Pharmaceutical Sciences Corneal-PAMPA : A novel, non-cell-based assay for prediction of corneal drug permeability. Eur. J. Pharm. Sci. 128 (November 2018), 232–239. https://doi.org/10.1016/j.ejps.2018.12.012.

Di Prima, G., Licciardi, M., Carfì Pavia, F., Lo Monte, A.I., Cavallaro, G., Giammona, G., 2019. Microfibrillar polymeric ocular inserts for triamcinolone acetonide delivery. Int. J. Pharm. 567 (June), 118459 https://doi.org/10.1016/j.ijpharm.2019.118459.

Dodero, A., Schlatter, G., Hébraud, A., Vicini, S., Castellano, M., 2021. Polymer-free cyclodextrin and natural polymer-cyclodextrin electrospun nanofibers: A comprehensive review on current applications and future perspectives. Carbohydr. Polym. 264 (April) https://doi.org/10.1016/j.carbpol.2021.118042.

Dumortier, G., Grossiord, J.L., Agnely, F., Chaumeil, J.C., 2006. A review of poloxamer 407 pharmaceutical and pharmacological characteristics. Pharm. Res. 23 (12), 2709–2728. https://doi.org/10.1007/s11095-006-9104-4.

Ellakwa, T.E., Fahmy, A., Ellakwa, D.E., 2017. Influence of poloxmer on the dissolution properties of mosapride and its pharmaceutical tablet formulation. Egypt. J. Chem. 60 (3), 443–451. https://doi.org/10.21608/EJCHEM.2017.3685.

Fan, J., Li, G., Deng, S., Wang, Z., 2019. Mechanical properties and microstructure of polyvinyl alcohol (PVA) modified cement mortar. Applied Sciences (switzerland) 9 (11). https://doi.org/10.3390/app9112178.

Galgatte, U.C., Chaudhari, P.D., 2014. Preformulation study of poloxamer 407 gels: Effect of additives. Int J Pharm Pharm Sci 6 (1), 130–133.

García-Millán, E., Quintáns-Carballo, M., Otero-Espinar, F.J., 2017. Solid-state characterization of triamcinolone acetonide nanosuspensiones by X-ray spectroscopy, ATR Fourier transforms infrared spectroscopy and differential scanning calorimetry analysis. Data Brief 15, 133–137. https://doi.org/10.1016/j.dib.2017.09.002.

Grimaudo, M.A., Nicoli, S., Santi, P., Concheiro, A., Alvarez-Lorenzo, C., 2018. Cyclosporine-loaded cross-linked inserts of sodium hyaluronan and hydroxypropyl-β-cyclodextrin for ocular administration. Carbohydr. Polym. 201 (August), 308–316. https://doi.org/10.1016/j.carbpol.2018.08.073.

Haider, A., Haider, S., Kang, I.K., 2018. A comprehensive review summarizing the effect of electrospinning parameters and potential applications of nanofibers in biomedical and biotechnology. Arab. J. Chem. 11 (8), 1165–1188. https://doi.org/10.1016/j.arabjc.2015.11.015.

He, Z., Wang, Z., Zhang, H., Pan, X., Su, W., Liang, D., Wu, C., 2011. Doxycycline and hydroxypropyl-β-cyclodextrin complex in poloxamer thermal sensitive hydrogel for ophthalmic delivery. Acta Pharm. Sin. B 1 (4), 254–260. https://doi.org/10.1016/j.apsb.2011.10.004.

Kaur, S., Sarma, P., Kaur, H., Prajapat, M., Shekhar, N., Bhattacharyya, J., Kaur, H., Kumar, S., Medhi, B., Ram, J., Das, D., Avti, P., Prakash, A., Singh, R., Bhattacharyya, A., 2021. Efficacy and Safety of Topical Cysteamine in Corneal Cystinosis: A Systematic Review and Meta-Analysis. Am. J. Ophthalmol. 223, 275–285. https://doi.org/10.1016/j.ajo.2020.07.052.

Kazsoki, A., Palcsó, B., Omer, S. M., Kovacs, Z., & Zelkó R (2022). Formulation of Levocetirizine-Loaded Core – Shell Type Nanofibrous Orally Dissolving Webs as a Potential Alternative for Immediate Release Dosage Forms. *Pharmaceutics*. https://www.mdpi.com/1999-4923/14/7/1442.

Kazsoki, A., Palcsó, B., Alpár, A., Snoeck, R., Andrei, G., Zelkó, R., 2021. Formulation of acyclovir (core)-dexpanthenol (sheath) nanofibrous patches for the treatment of herpes labialis. Int. J. Pharm. 611 https://doi.org/10.1016/j.ijpharm.2021.121354.

Kesavan, K., Kant, S., Singh, P.N., Pandit, J.K., 2011. Effect of hydroxypropyl-β-cyclodextrin on the ocular bioavailability of dexamethasone from a pH-induced mucoadhesive hydrogel. Curr. Eye Res. 36 (10), 918–929. https://doi.org/10.3109/02713683.2011.593728.

Kharazmi, A., Faraji, N., Hussin, R.M., Saion, E., Yunus, W.M.M., Behzad, K., 2015. Structural, optical, opto-thermal and thermal properties of ZnS-PVA nanofluids synthesized through a radiolytic approach. Beilstein J. Nanotechnol. 6 (1), 529–536. https://doi.org/10.3762/bjnano.6.55.

Lakhani, P., Patil, A., Taskar, P., Ashour, E., Majumdar, S., 2020. Curcumin-loaded Nanostructured Lipid Carriers for Ocular Drug Delivery: Design Optimization and Characterization. J Drug Deliv Sci Technol. 662, 159–166. https://doi.org/10.1016/j.jddst.2018.07.010.Curcumin-loaded.

Laurano, R., Abrami, M., Grassi, M., Ciardelli, G., Boffito, M., Chiono, V., 2020. Using Poloxamer® 407 as Building Block of Amphiphilic Poly(ether urethane)s: Effect of its Molecular Weight Distribution on Thermo-Sensitive Hydrogel Performances in the Perspective of Their Biomedical Application. Front. Mater. 7 (November), 1–15. https://doi.org/10.3389/fmats.2020.594515.

Liang, H., Labbé, A., Baudouin, C., Plisson, C., Giordano, V., 2021. Long-term follow-up of cystinosis patients treated with 0.55% cysteamine hydrochloride. Br. J. Ophthalmol. 105 (5), 608–613. https://doi.org/10.1136/bjophthalmol-2020-316450.

Loftsson, T., Vogensen, S.B., Brewster, M.E., 2007. Effects of Cyclodextrins on Drug Delivery Through Biological Membranes. J. Pharm. Sci. 96 (10), 2532–2546. https://doi.org/10.1002/jps.

Lorenzo-Veiga, B., Sigurdsson, H.H., Loftsson, T., 2019. Nepafenac-loaded cyclodextrin/polymer nanoaggregates: A new approach to eye drop formulation. Materials 12 (2). https://doi.org/10.3390/ma12020229.

Lorenzo-Veiga, B., Diaz-Rodriguez, P., Alvarez-Lorenzo, C., Loftsson, T., Sigurdsson, H. H., 2020. In Vitro and Ex Vivo Evaluation of Nepafenac-Based Cyclodextrin Microparticles for Treatment of Eye Inflammation. Nanomaterials 10 (4). https://doi.org/10.3390/nano10040709.

Luepke, N.P., 1985. Hen's egg chorioallantoic membrane test for irritation potential. Food Chem. Toxicol. 23 (2), 287–291. https://doi.org/10.1016/0278-6915(85)90030-4.

MacHín, R., Isasi, J.R., Vélaz, I., 2012. β-Cyclodextrin hydrogels as potential drug delivery systems. Carbohydr. Polym. 87 (3), 2024–2030. https://doi.org/10.1016/j.carbpol.2011.10.024.

Maharjan, P., Cho, K.H., Maharjan, A., Shin, M.C., Moon, C., Min, K.A., 2019. Pharmaceutical challenges and perspectives in developing ophthalmic drug formulations. J. Pharm. Investig. 49 (2), 215–228. https://doi.org/10.1007/s40005-018-0404-6.

Mansur, H.S., Sadahira, C.M., Souza, A.N., Mansur, A.A.P., 2008. FTIR spectroscopy characterization of poly (vinyl alcohol) hydrogel with different hydrolysis degree and chemically crosslinked with glutaraldehyde. Mater. Sci. Eng. C 28 (4), 539–548. https://doi.org/10.1016/j.msec.2007.10.088.

Mecozzi, M., Sturchio, E., 2017. Computer assisted examination of infrared and near infrared spectra to assess structural and molecular changes in biological samples exposed to pollutants: A case of study. *Journal of*. Imaging 3 (1). https://doi.org/10.3390/jimaging3010011.

Mehta, P., Al-Kinani, A.A., Arshad, M.S., Chang, M.W., Alany, R.G., Ahmad, Z., 2017. Development and characterisation of electrospun timolol maleate-loaded polymeric contact lens coatings containing various permeation enhancers. Int. J. Pharm. 532 (1), 408–420. https://doi.org/10.1016/j.ijpharm.2017.09.029.

Meireles, A.B., Corrêa, D.K., da Silveira, J.V.W., Millás, A.L.G., Bittencourt, E., de Brito-Melo, G.E.A., González-Torres, L.A., 2018. Trends in polymeric electrospun fibers and their use as oral biomaterials. In. Exp. Biol. Med. Vol. 243(8, 665–676. https://doi.org/10.1177/1535370218770404.

Miranda, G.M., Santos, R.E., V. O., Bessa, J. R., Teles, Y. C. F., Yahouédéhou, S. C. M. A., Goncalves, M. S., & Ribeiro-Filho, J., 2021. Inclusion complexes of non-steroidal anti-inflammatory drugs with cyclodextrins: A systematic review. Biomolecules 11 (3), 1–24. https://doi.org/10.3390/biom11030361.

Pandit, J., Chaudhary, N., Emad, N.A., Ahmad, S., Solanki, P., Aqil, M., Sultana, Y., Solanki, P., 2023. Fenofibrate loaded nanofibers based thermo-responsive gel for ocular delivery: Formulation development, characterization and in vitro toxicity study. J. Drug Delivery Sci. Technol. 89 (July), 104935 https://doi.org/10.1016/j.jddst.2023.104935.

Pascolini, D., Mariotti, S.P., 2012. Global estimates of visual impairment: 2010. Br. J. Ophthalmol. 96 (5), 614–618. https://doi.org/10.1136/bjophthalmol-2011-300539.

Pinxten, A.M., Hua, M.T., Simpson, J., Hohenfellner, K., Levtchenko, E., Casteels, I., 2017. Clinical Practice: A Proposed Standardized Ophthalmological Assessment for Patients with Cystinosis. Ophthalmol Therapy 6 (1), 93–104. https://doi.org/10.1007/s40123-017-0089-3.

Polat, H.K., Bozdağ Pehlivan, S., Özkul, C., Çalamak, S., Öztürk, N., Aytekin, E., Fırat, A., Ulubayram, K., Kocabeyoğlu, S., İrkeç, M., Çalış, S., 2020a. Development of besifloxacin HCl loaded nanofibrous ocular inserts for the treatment of bacterial keratitis: In vitro, ex vivo and in vivo evaluation. Int. J. Pharm. 585 (April) https://doi.org/10.1016/j.ijpharm.2020.119552.

Polat, H.K., Bozdağ Pehlivan, S., Özkul, C., Çalamak, S., Öztürk, N., Aytekin, E., Fırat, A., Ulubayram, K., Kocabeyoğlu, S., İrkeç, M., Çalış, S., 2020b. Development of besifloxacin HCl loaded nanofibrous ocular inserts for the treatment of bacterial keratitis: In vitro, ex vivo and in vivo evaluation. Int. J. Pharm. 585 (June) https://doi.org/10.1016/j.ijpharm.2020.119552.

Pourtalebi Jahromi, L., Ghazali, M., Ashrafi, H., Azadi, A., 2020. A comparison of models for the analysis of the kinetics of drug release from PLGA-based nanoparticles. Heliyon 6 (2). https://doi.org/10.1016/j.heliyon.2020.e03451.

Rajput, S., Shrimali, C., Baghel, M., 2015. Development and validation of UV and RP-HPLC method for estimation of Nepafenac in bulk drug and opthalmic formulation. Journal of Advanced Pharmacy Education & Research 5 (1), 1–20.

Russo, E., Villa, C., 2019. Poloxamer hydrogels for biomedical applications. Pharmaceutics 11 (12). https://doi.org/10.3390/pharmaceutics11120671.

Shelley, H., Grant, M., Smith, F.T., Abarca, E.M., Jayachandra Babu, R., 2018. Improved Ocular Delivery of Nepafenac by Cyclodextrin Complexation. AAPS PharmSciTech 19 (6), 2554–2563. https://doi.org/10.1208/s12249-018-1094-0.

Singla, J., Bajaj, T., Goyal, A.K., Rath, G., 2019. Development of Nanofibrous Ocular Insert for Retinal Delivery of Fluocinolone Acetonide. Curr. Eye Res. 44 (5), 541–550. https://doi.org/10.1080/02713683.2018.1563196.

Thakkar, R., Komanduri, N., Dudhipala, N., Tripathi, S., Repka, M.A., Majumdar, S., 2021. Development and optimization of hot-melt extruded moxifloxacin hydrochloride inserts, for ocular applications, using the design of experiments. Int. J. Pharm. 603 (January), 120676 https://doi.org/10.1016/j.ijpharm.2021.120676.

Tighsazzadeh, M., Mitchell, J.C., Boateng, J.S., 2019. Development and evaluation of performance characteristics of timolol- loaded composite ocular fi lms as potential delivery platforms for treatment of glaucoma. Int. J. Pharm. 566 (May), 111–125. https://doi.org/10.1016/j.ijpharm.2019.05.059.

Topal, B., Çetin Altindal, D., Gümüsderelioglu, M., 2015. Melatonin/HPβCD complex: Microwave synthesis, integration with chitosan scaffolds and inhibitory effects on MG-63CELLS. Int. J. Pharm. 496 (2), 801–811. https://doi.org/10.1016/j.ijpharm.2015.11.028.

Vincze, A., Facskó, R., Budai-Szűcs, M., Katona, G., Gyarmati, B., Csorba, A., Zelkó, R., Nagy, Z.Z., Szente, L., Balogh, G.T., 2023. Cyclodextrin-enabled nepafenac eye drops with improved absorption open a new therapeutic window. Carbohydr. Polym. 310 (February) https://doi.org/10.1016/j.carbpol.2023.120717.

Wagh, D., Shahi, S.R., Dabir, P.D., Deore, W., 2017. Spectrophotometric Method for the Determination of Nepafenac in Opthalmic Formulation. World J. Pharm. Res. 6 (6), 623–630. https://doi.org/10.20959/wjpr20176-8410.

Yasser, M., Teaima, M., El-Nabarawi, M., El-Monem, R.A., 2019. Cubosomal based oral tablet for controlled drug delivery of telmisartan: formulation, in-vitro evaluation and in-vivo comparative pharmacokinetic study in rabbits. Drug Dev. Ind. Pharm. 45 (6), 981–994. https://doi.org/10.1080/03639045.2019.1590392.